Quasi-free photoproduction of η-mesons off the deuteron

I. Jaegle[1], B. Krusche[1], A.V. Anisovich[2,3], J.C.S. Bacelar[4], B. Bantes[5], O. Bartholomy[2], D.E. Bayadilov[2,3], R. Beck[2], Y.A. Beloglazov[3], R. Castelijns[4], V. Crede[2,6], M. Dieterle[1], H. Dutz[5], D. Elsner[5], R. Ewald[5], F. Frommberger[5], C. Funke[2], R. Gothe[5,8], R. Gregor[7], A.B. Gridnev[3], E. Gutz[2], W. Hillert[5], S. Höffgen[5], P. Hoffmeister[2], I. Horn[2], J. Junkersfeld[2], H. Kalinowsky[2], S. Kammer[5], I. Keshelashvili[1], V. Kleber[5], Frank Klein[5], Friedrich Klein[5], E. Klempt[2], M. Konrad[5], M. Kotulla[1], M. Lang[2], H. Löhner[4], I.V. Lopatin[3], S. Lugert[7], Y. Maghrbi[1], D. Menze[5], T. Mertens[1], J.G. Messchendorp[4], V. Metag[7], V.A. Nikonov[2,3], M. Nanova[7], D.V. Novinski[2,3], R. Novotny[7], M. Ostrick[5,9], L.M. Pant[7,10], H. van Pee[2,7], M. Pfeiffer[7], F. Pheron[1], A. Roy[7,11], A.V. Sarantsev[2,3], S. Schadmand[7,12], C. Schmidt[2], H. Schmieden[5], B. Schoch[5], S.V. Shende[4], V. Sokhoyan[2], A. Süle[5], V.V. Sumachev[3], T. Szczepanek[2], U. Thoma[2,7], D. Trnka[7], R. Varma[7,11], D. Walther[5], C. Wendel[2], D. Werthmüller[1], and L. Witthauer[1]
(The CBELSA/TAPS collaboration)

[1] Departement Physik, Universität Basel, Switzerland
[2] Helmholtz-Institut für Strahlen- und Kernphysik der Universität Bonn, Germany
[3] Petersburg Nuclear Physics Institute, Gatchina, Russia
[4] KVI, University of Groningen, The Netherlands
[5] Physikalisches Institut der Universität Bonn, Germany
[6] Department of Physics, Florida State University, Tallahassee, USA
[7] II. Physikalisches Institut, Universität Giessen, Germany
[8] present address: University of South Carolina, USA
[9] present address: University of Mainz, Germany
[10] on leave from Nucl. Phys. Division, BARC, Mumbai, India
[11] on leave from Department of Physics, Indian Institute of Technology Mumbai, India
[12] present address: Institut für Kernphysik, Forschungszentrum Jülich, Germany

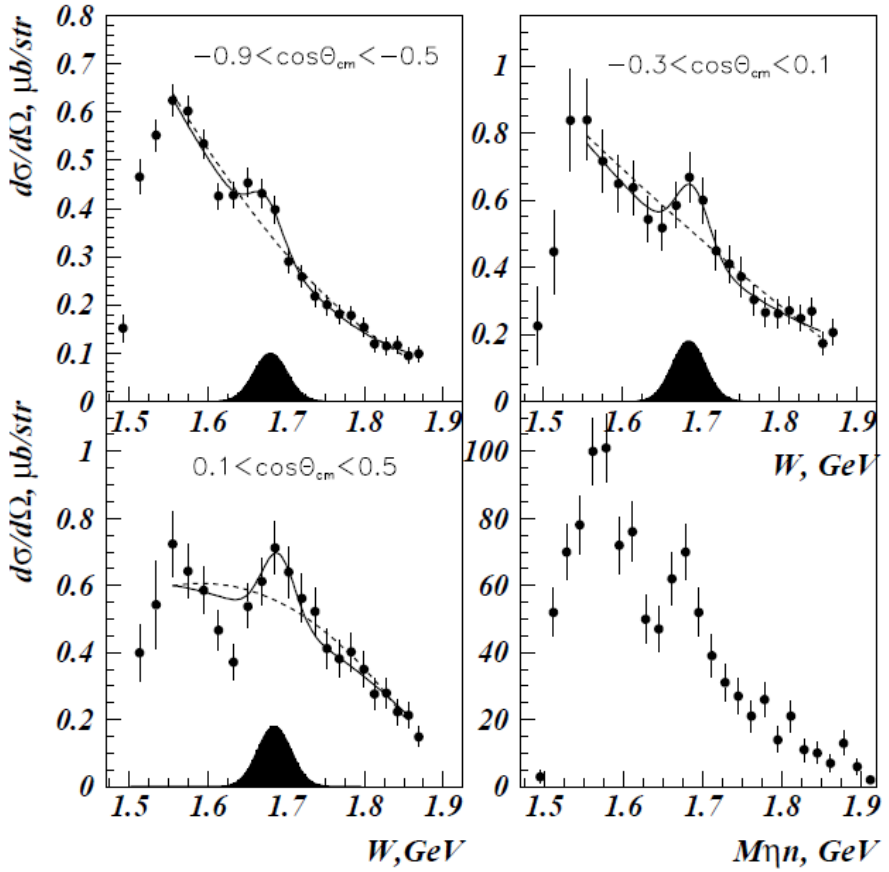

Fig. 1. Quasi-free cross sections and ηn invariant mass spectrum (low right panel) for the $\gamma n \to \eta n$ reaction (data from [13]). Solid lines are the fit by the sum of 3-order polynomial and narrow state. Dashed lines are the fit by 3-order polynomial only. Dark areas show the simulated signal of a narrow state.

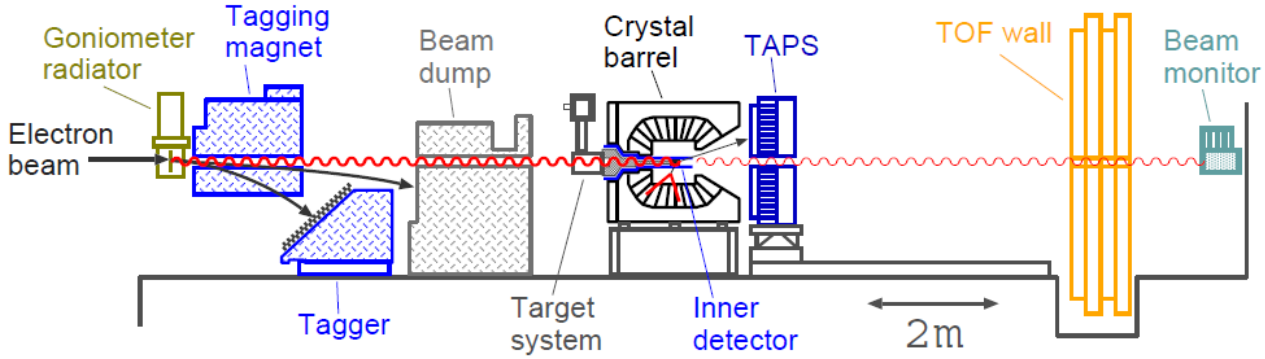

Fig. 2. Overview of the experimental setup. The electron beam enters from the left side. Scattered electrons were detected in the counters of the tagging spectrometer (cf. Fig. 3). The liquid deuterium target was mounted in the center of the Crystal Barrel. The forward range was covered by the TAPS detector. The Time-of-flight wall was mounted, but not used in the experiment. Beam intensity was monitored at the end of the beam line.

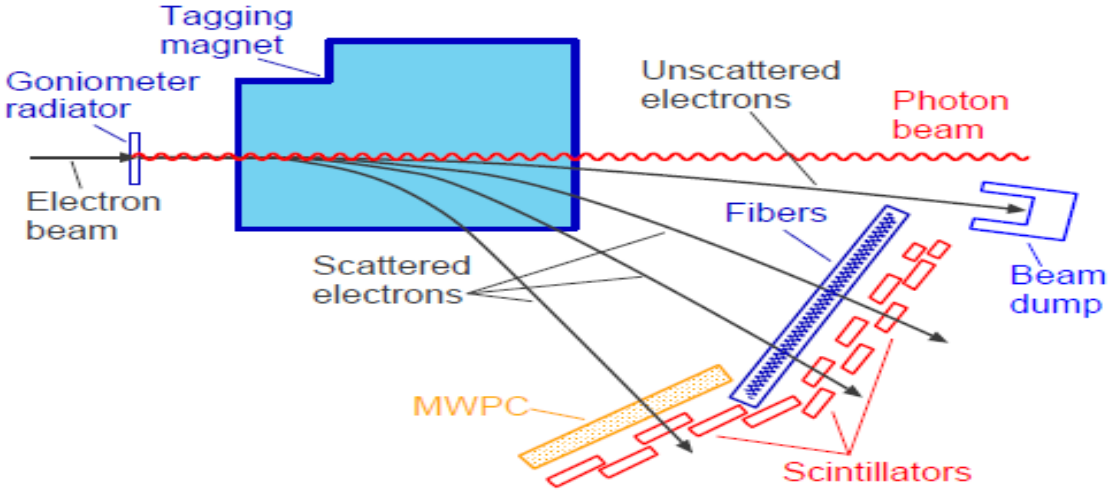

Fig. 3. Setup of the tagging spectrometer. Unscattered electrons stop in the beam-dump. Scattered electrons pass a two layer detection system. Scintillating fiber detectors (good position resolution) and scintillator bars (good time resolution) cover photon energies up to 80 % of the electron beam energy. The part covered by a multiple wire chamber (MWPC) (low energy electrons corresponding to photon energies above 80 % of the electron beam energy) was not used in the experiment.

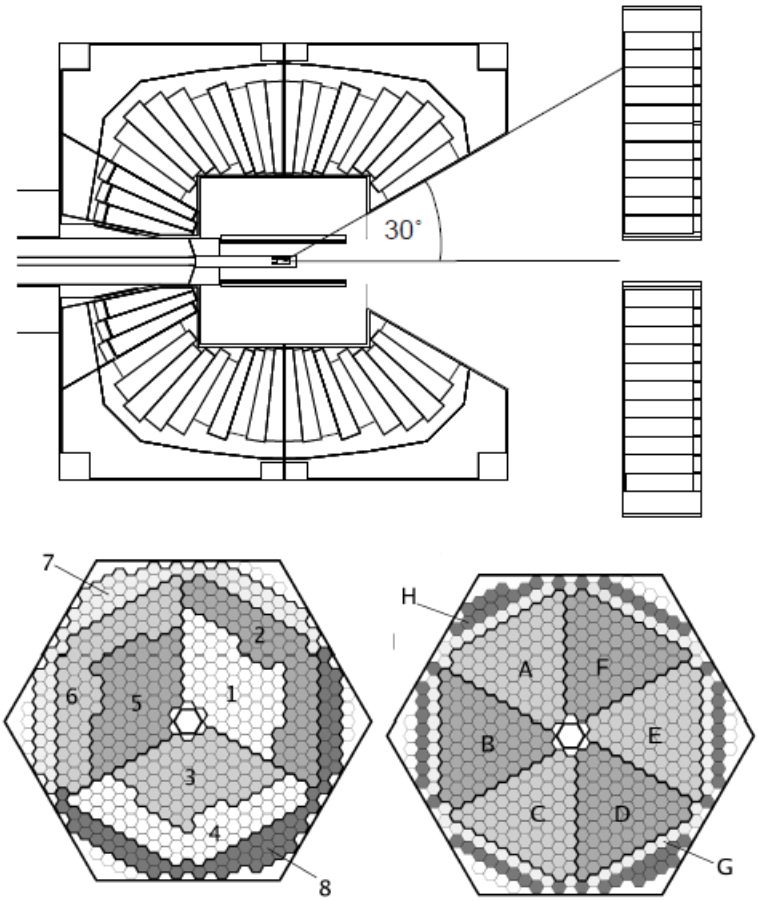

Fig. 4. Arrangement of the Crystal Barrel and TAPS detectors. Upper part: side view, lower part: front view of the TAPS wall: left hand side: logical segmentation for the LED-low trigger, right hand side: logical segmentation for the LED-high trigger (see text).

This component was made of 528 BaF_2 crystals of hexagonal shape with an inner diameter of 5.9 cm and a length of 25 cm corresponding to 12 X_o. They were arranged in a wall-like structure as shown in the lower part of Fig. 4, covering polar angles down to 4.5°. The front face of the BaF_2 wall was located 1.18 m from the center of the target.

The two calorimeters have a comparable energy resolution [58,60]

$$\frac{\sigma_E}{E} \approx \frac{2-3\%}{\sqrt[4]{E/GeV}} \quad . \tag{4}$$

These events were subjected to a combined invariant and missing mass analysis. In the first step of the invariant mass analysis the invariant masses of all combinations of three disjunct pairs of neutral hits were calculated. In the case of six neutral hits (events with proton candidate or without candidate for recoil nucleon) these are 15 different combinations among which the 'best' combination was chosen by a χ^2-test, minimizing

$$\chi^2 = \sum_{k=1}^{3} \frac{(m_k(\gamma\gamma) - m_{\pi^0})^2}{(\Delta m_k(\gamma\gamma))^2} \tag{6}$$

for all disjunct combinations where m_{π^0} is the pion mass and the $m_{\gamma\gamma}$ are the invariant masses of the photon pairs with their uncertainties $\Delta m_{\gamma\gamma}$ calculated for each photon pair from the energy and angular resolution of the detector. For events with seven neutral hits (events with neutron candidate) one must in addition loop over the unpaired hit giving rise to 105 combinations. Once the 'best' combination was determined, in all cases a cut between 110 MeV - 160 MeV was applied to the invariant masses. Only events where all three pairs of the best combination passed this cut were kept. Subsequently, for events with seven neutral hits, the residual hit was taken as neutron candidate.

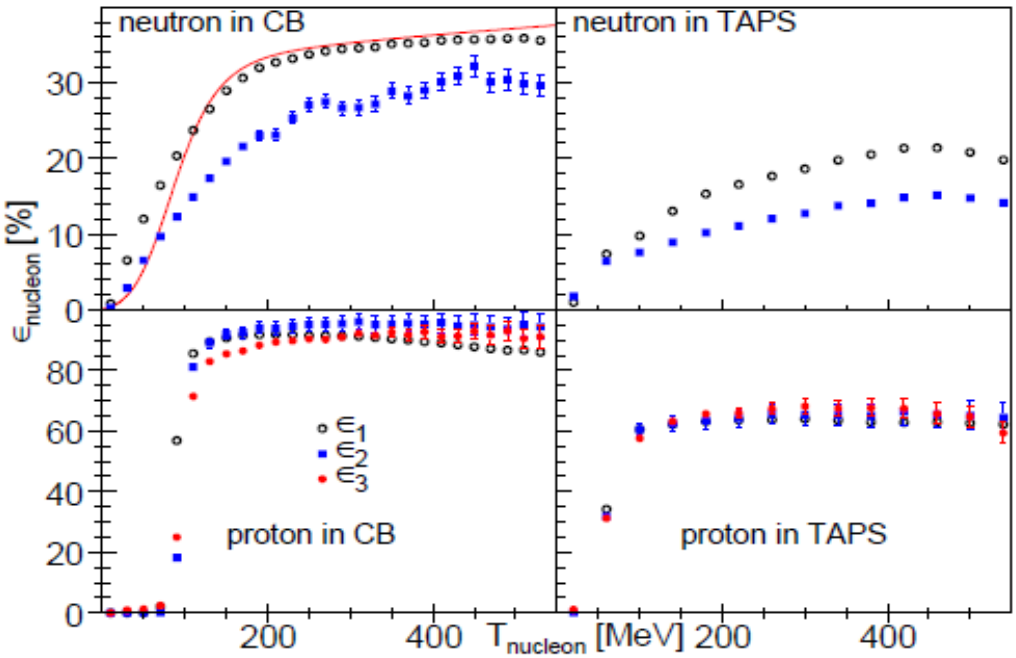

Fig. 10. Detection efficiency for recoil nucleons. Upper row: neutrons, lower row protons, left hand side: Crystal Barrel, right hand side: TAPS. For all figures: ϵ_1 (open black circles): MC simulation for isotropically emitted nucleons without further detector hits, ϵ_2 (blue squares): simulation with six decay photons from η-meson decays, ϵ_3 (red dots): experimentally determined proton detection efficiency from η and $2\pi^0$ photoproduction from proton (hydrogen) target (see text). Solid (red)line: measured neutron detection efficiency for CB at CERN [64].

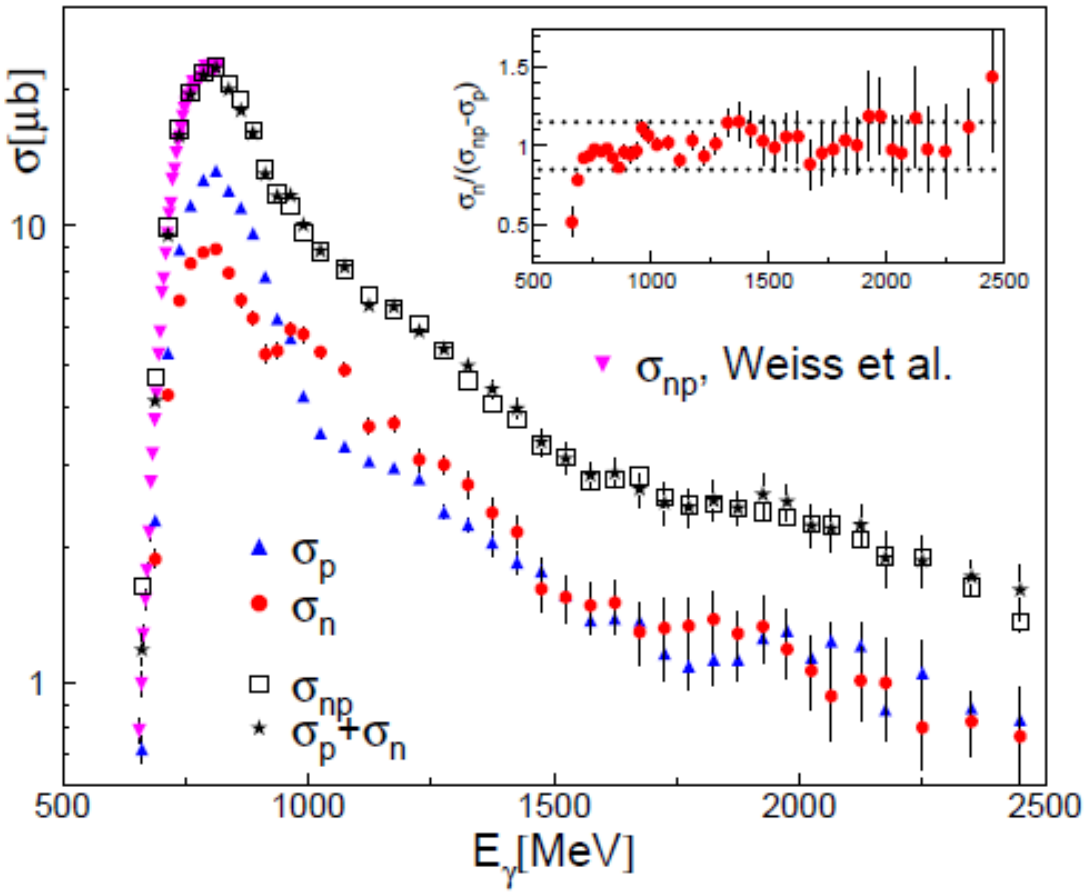

Fig. 14. Comparison of total cross sections. (Blue) upward triangles: quasi-free proton cross section σ_p, (red) dots: quasi-free neutron cross section σ_n, (black) open squares: inclusive quasi-free cross section σ_{np}, (black) stars: $\sigma_n + \sigma_p$. Downward (magenta) triangles: inclusive quasi-free cross section from Weiss et al. [39]. Insert: ratio of neutron cross sections.

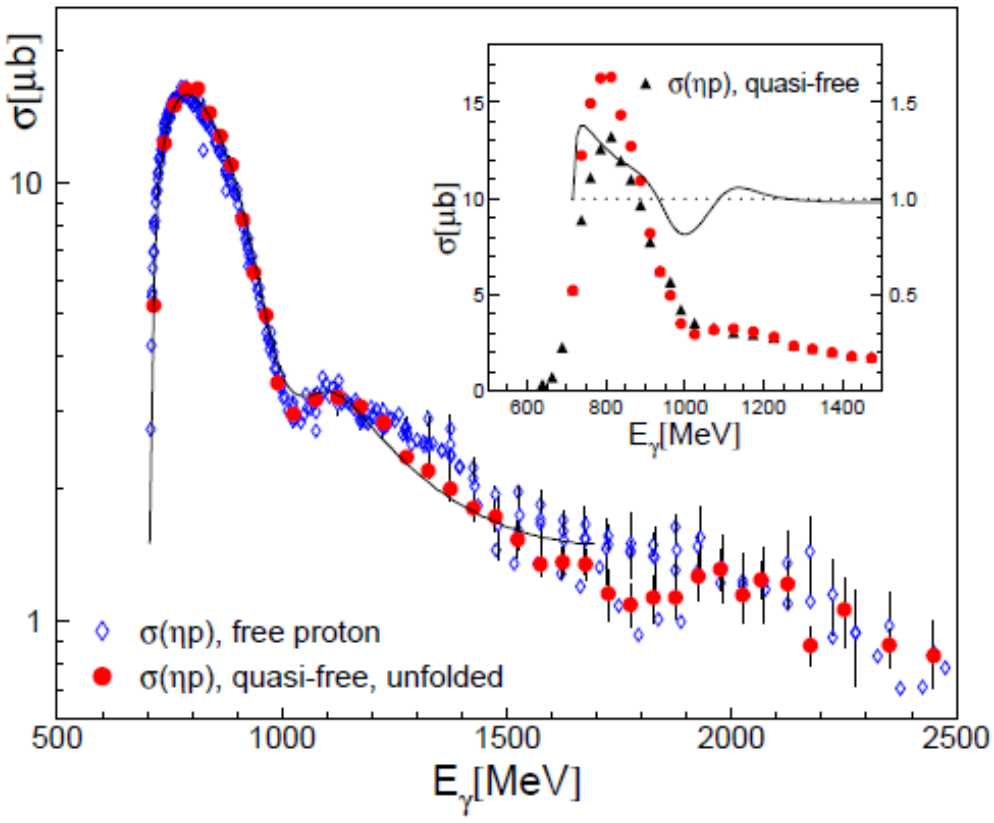

Fig. 17. Comparison of the total cross section of quasi-free production off the bound proton to free proton data. Filled (red) circles: quasi-free σ_p corrected for effects of Fermi motion (see text). Open (blue) diamonds: free proton data from [16, 21–23, 28, 29, 31]. Total cross sections for the free proton data from [22, 29] have been estimated from the published differential cross sections. Solid line: eta-Maid model [34]. Insert: comparison of quasi-free proton data (black triangles) to quasi-free proton data after correction of Fermi motion effects (red filled circles) (see text). Solid curve: ratio of free and folded cross section (scale at right hand side).

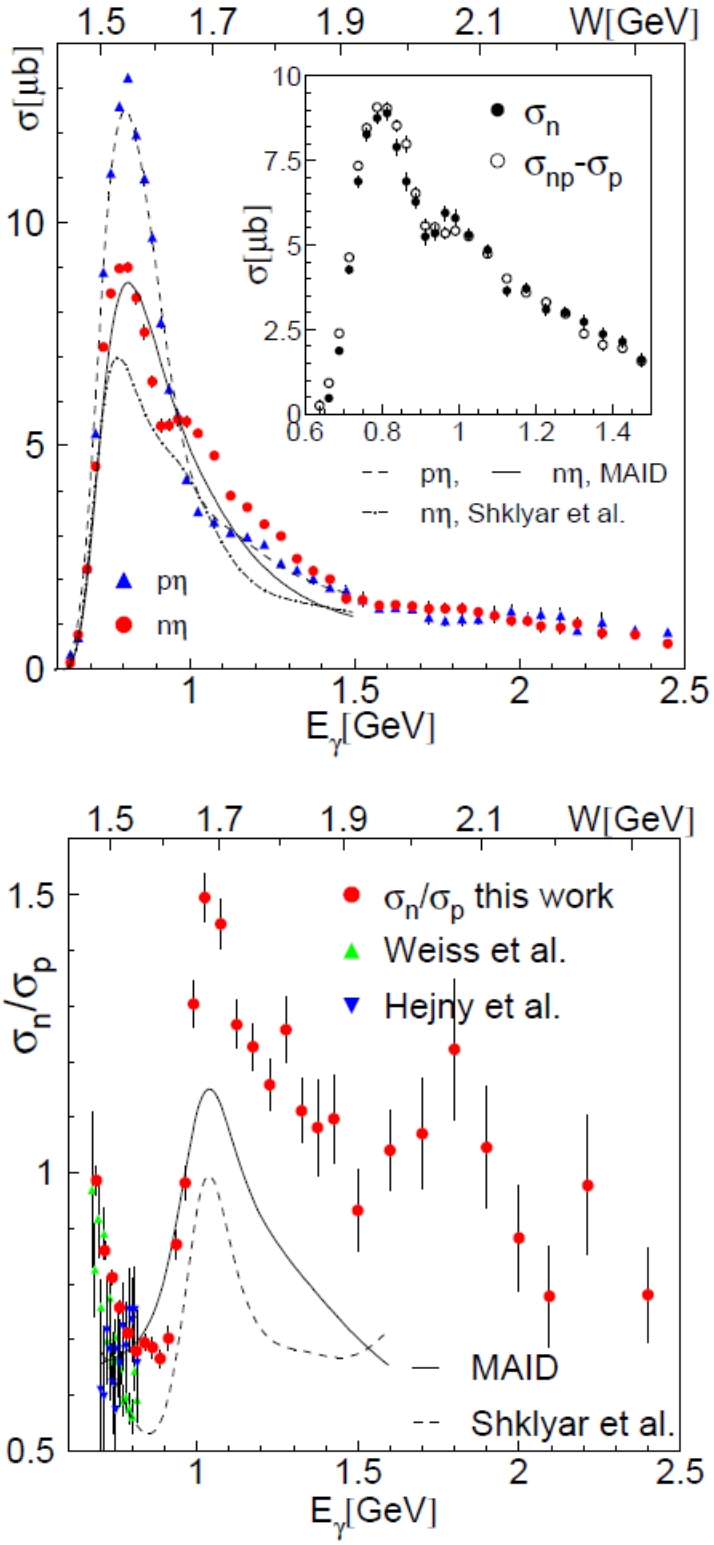

Fig. 19. Comparison of quasi-free proton and neutron excitation function. Upper part: Curves model results, dashed: Eta-MAID for proton [34], solid: Eta-MAID for neutron [34], dash-dotted: Shklyar et al. [50]. Insert: comparison of the total neutron cross sections extracted from the coincident measurement of neutrons (σ_n) and the difference of inclusive and proton data (σ'_n). Bottom part: Cross section ratio σ_n/σ_p compared to previous data from quasi-free production off the deuteron [39] and off ^{4}He [38] and model results (solid: MAID [34], dashed: Shklyar et al. [50]) folded with Fermi motion.

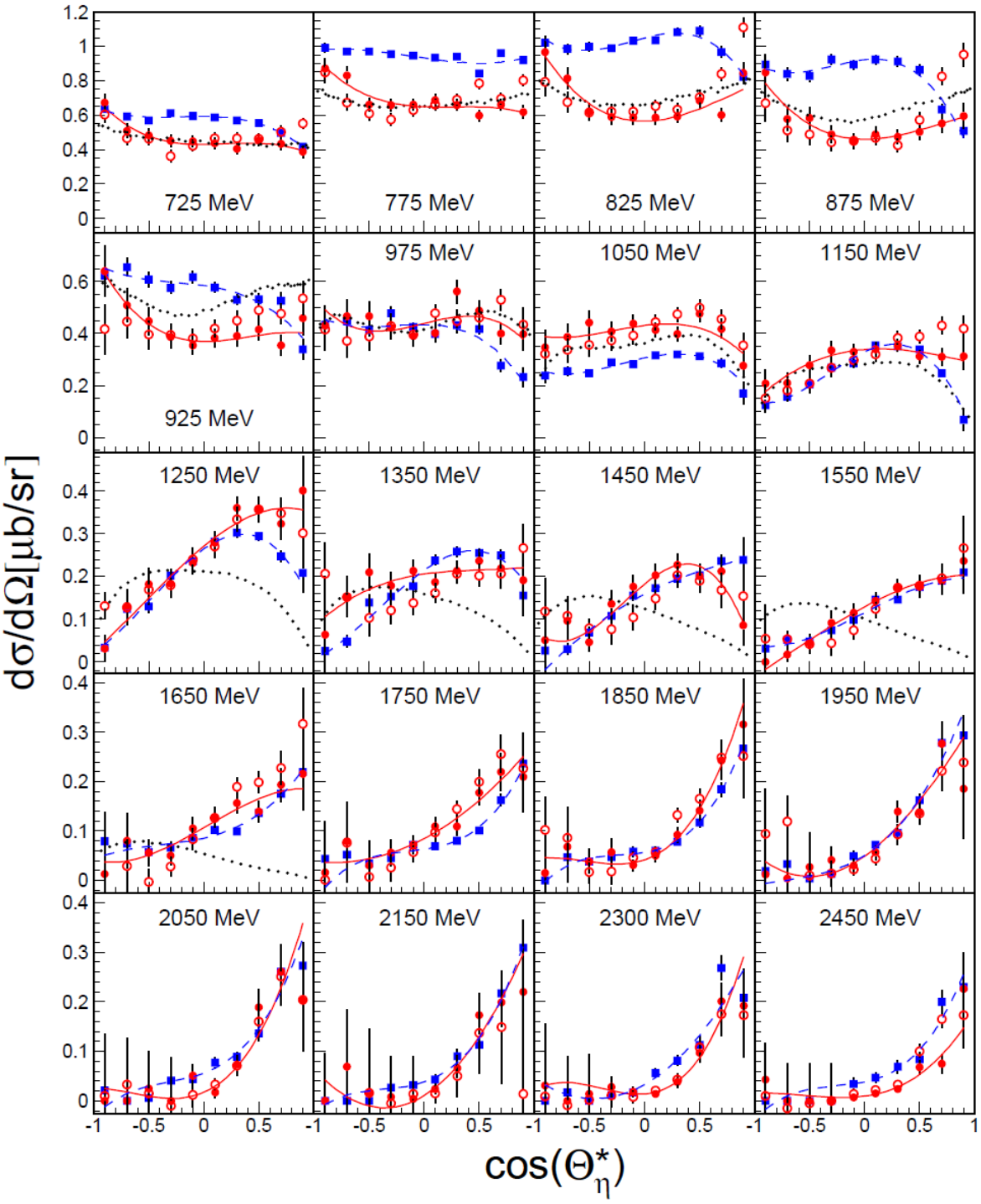

Fig. 20. Quasi-free angular distributions, labels indicate incident photon energy. (Blue) squares: proton coincidence σ_p, (red) filled circles: neutron coincidence σ_n, (red) open circles: difference of inclusive and proton σ'_n. Dashed (blue) curves: fit of proton data, solid (red) curves: fit of neutron data, dotted (black) curves: Eta-MAID for neutron folded with Fermi motion.

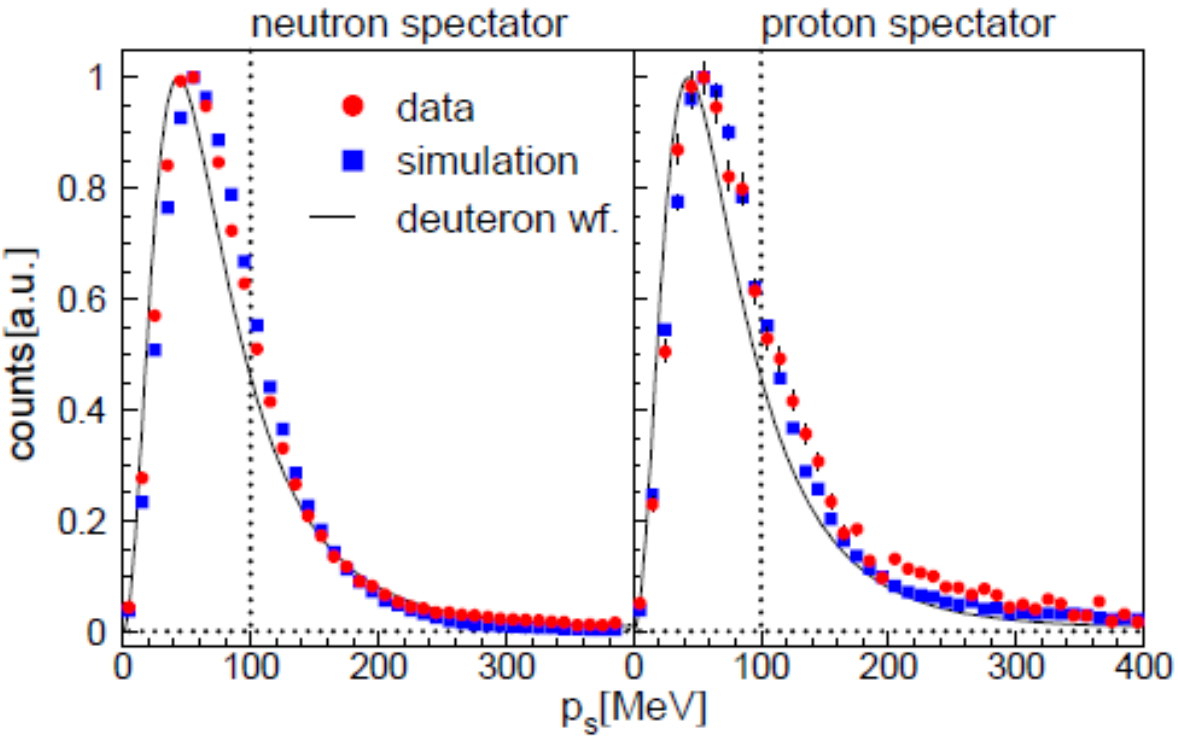

Fig. 22. Momentum distributions of spectator nucleons. (Red) dots: reconstructed from data, (black) lines: expected from deuteron wave function [68], (blue) squares: Monte Carlo simulation including detector response. Left hand side: neutron spectator (i.e. recoil proton detected), right hand side: proton spectator (i.e. recoil neutron detected).

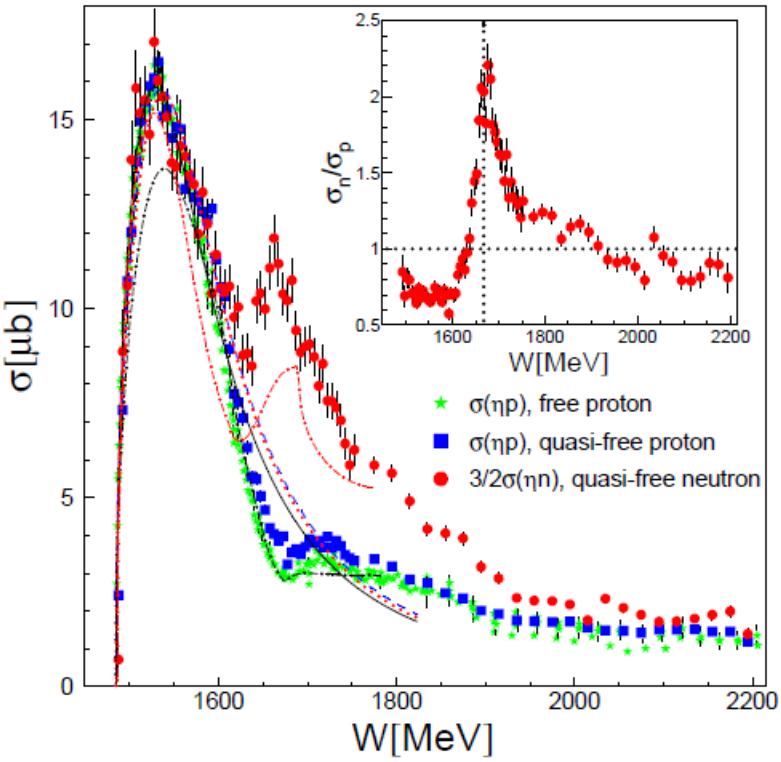

Fig. 23. Total cross sections as function of final state invariant mass W without cut on spectator momentum. (Red) dots: quasi-free neutron, (blue) squares: quasi-free proton, (green) stars: free proton data. Curves: fitted (up to $W = 1600$ MeV) $S_{11}(1535)$ line shapes. (Black) solid: free proton, (blue) dashed: quasi-free proton, (red) dotted: quasi-free neutron. Insert: ratio of quasi-free neutron - proton data. Dash-dotted curves: model results from [49].

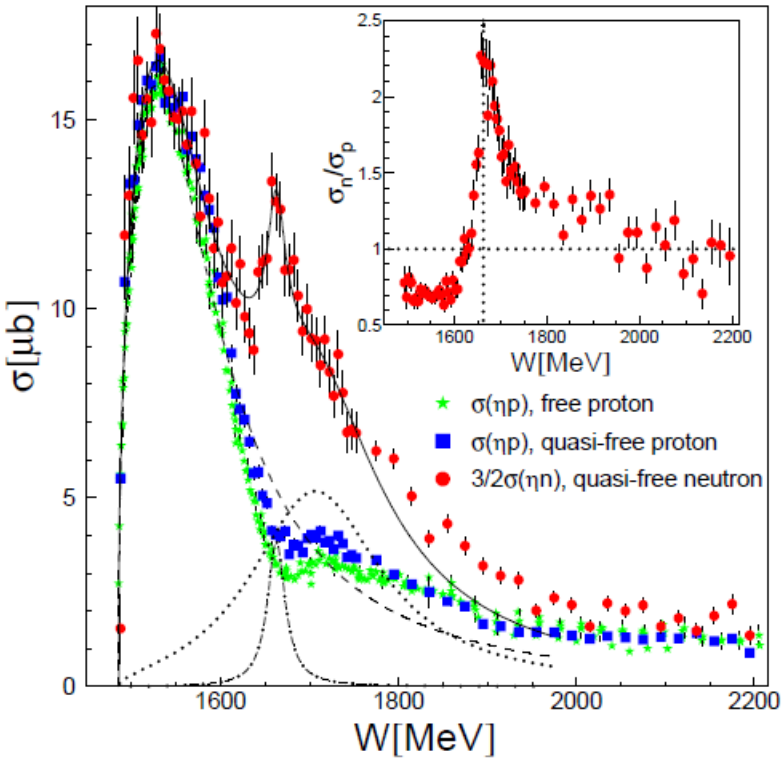

Fig. 24. Total cross sections as function of final state invariant mass W for spectator momenta $p_S < 100$ MeV. Notation as in Fig. 23. All curves for neutron data; dashed: fitted S_{11} line shape, dotted: broad Breit-Wigner resonance, dash-dotted: narrow Breit-Wigner, solid: sum of all.

Table 3. Result of Breit-Wigner fits. $N\eta$ branching ratio of S_{11} is assumed as b_η=0.5. Upper part of table: Comparison of fits of $S_{11}(1535)$ resonance for free proton, quasi-free proton, and quasi-free neutron data to PDG estimates [33] and BoGa model fit [53]. †: Breit-Wigner mass, in brackets pole position; ‡: only magnitudes, no signs; §: only pole positions given, no Breit-Wigner mass. Bottom part: fit of neutron data with S_{11}. resonance and two further Breit-Wigner curves. All uncertainties of fit parameters are statistical only.

$S_{11}(1535)$	$W^\dagger$ [MeV]	$\Gamma^\dagger$ [MeV]	$A^\ddagger_{1/2}$ [10^{-3}GeV$^{-1/2}$]
PDG	1535±10 (1510±10)	150±25 (170±80)	$A^p_{1/2}$: 90±30 $A^n_{1/2}$: 46±27
BoGa§	- (1505±20)	- (145±25)	$A^p_{1/2}$: 90±25 $A^n_{1/2}$: 80±20
$\gamma p \to p\eta$	1536±1	170±2	106±1
$\gamma d \to (n)p\eta$	1544±2	181±13	109±3
$\gamma d \to (p)n\eta$	1546±3	176±20	90±4
$\gamma d \to (p)n\eta$			
$S_{11}(1535)$	1535±4	166±23	88±6
'broad BW'	1701±15	180±35	-
'narrow BW'	1663±3	25±12	-

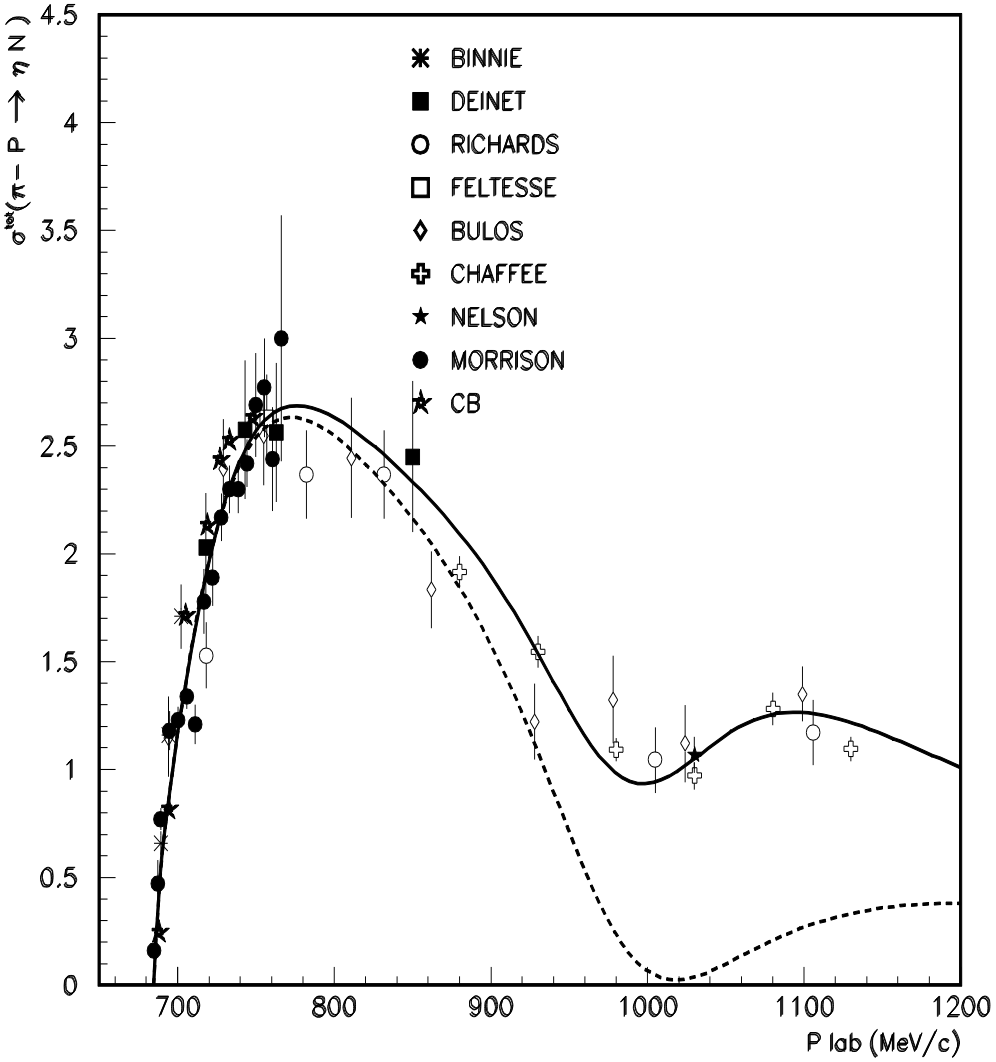

The S wave K-matrix for $\pi p \to \eta n$ transition in this region has the following form:

$$\frac{\alpha_{1\pi}\alpha_{1\eta}}{M_1 - w} + \frac{\alpha_{2\pi}\alpha_{2\eta}}{M_2 - w} + \text{non-resonance terms.} \tag{31}$$

It can be easy seen from this formula, that there exists an energy $M_1 < \omega_0 < M_2$ at which $K_{\pi\to\eta}(\omega_0) = 0$. Since the second $S_{11}(1650)$ resonance has a small branching ratio for the η decay, this energy must be close to $M_2 (P_{lab} \approx 980$ MeV/c).

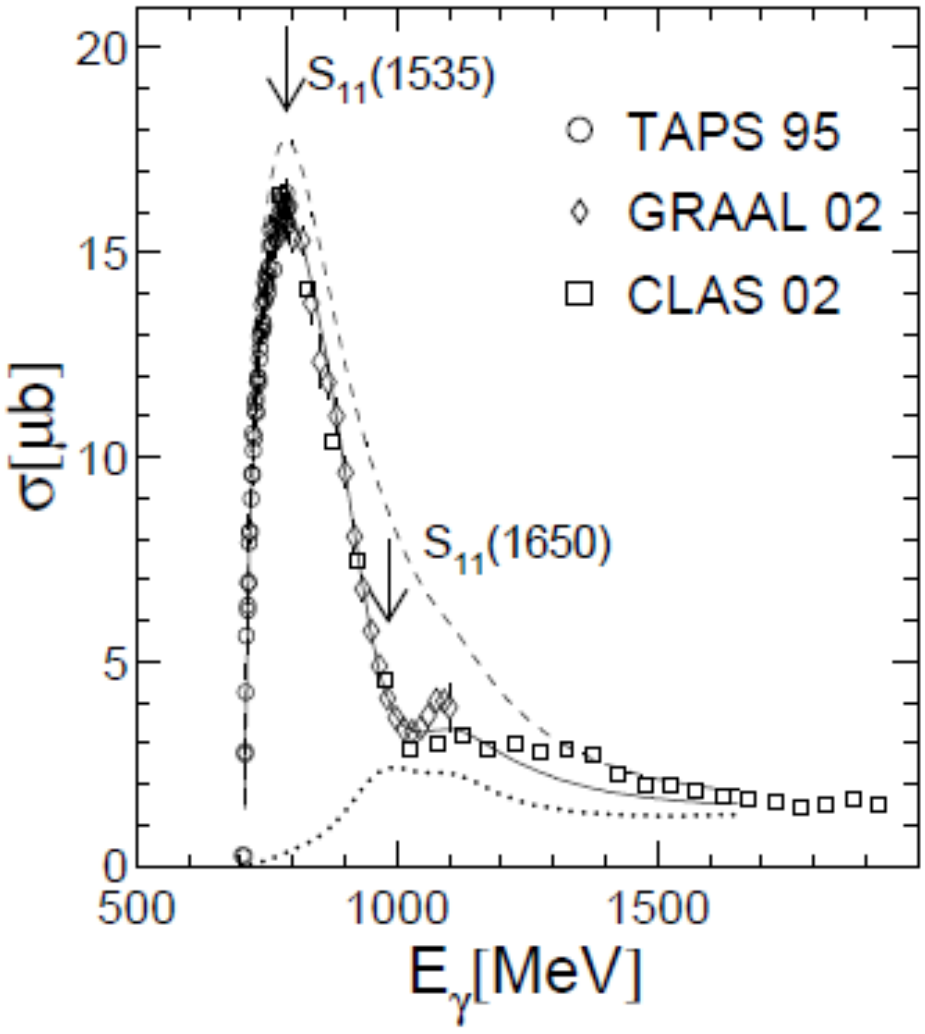
20
15
10
5
0
σ[μb]
500
1000
1500
E_γ[MeV]
S11(1535)
S11(1650)
TAPS 95
GRAAL 02
CLAS 02